

Optics Letters

Voltage-induced waveguides in lithium niobate films on silicon substrates

M. CHAUVET,^{1,*} P. THOA,¹ AND F. BASSIGNOT²

¹Department of Optics, FEMTO-ST Institute, UMR CNRS 6174, University of Bourgogne Franche-Comté, 15B Avenue des Montboucons, F-25000 Besançon, France

²Femto-Engineering, 15B Avenue des Montboucons, F-25000 Besançon, France

*Corresponding author: mathieu.chauvet@univ-fcomte.fr

Received 9 January 2017; revised 31 January 2017; accepted 5 February 2017; posted 9 February 2017 (Doc. ID 283927); published 2 March 2017

Electrically tunable channel waveguides have been fabricated by domain inversion of a LiNbO₃ thin film bonded to a silicon wafer. The electro-optic effect is used to induce the waveguides and to alter its guiding properties. A low amplitude electric signal can tune the voltage-induced structure from an efficient waveguide to an antiguid giving a waveguide transmission that varies over more than 25 dB. The frequency response of the components is given. © 2017 Optical Society of America

OCIS codes: (230.2090) Electro-optical devices; (130.3730) Lithium niobate; (130.4110) Modulators; (230.7370) Waveguides; (220.4000) Microstructure fabrication.

<https://doi.org/10.1364/OL.42.001019>

Waveguides whose properties can be modified with the application of an electric field are key elements to process optical signals. They are part of guided optics devices such as modulators, variable attenuators, and switches that rely on various physical phenomena. Among others, we can cite electroabsorption [1], thermal effect [2] or electro-optic effect [3,4]. The latter is, by far, the most widely used one thanks to its fast and nonresonant response. These electro-optic devices are usually made of permanent waveguides whose guiding properties are slightly altered by application of a voltage. However, the ability to make a waveguide appear or disappear at will could find applications. For instance, full control over coupled waveguide arrays would bring great flexibility to route and shape an input signal beam. Such voltage-induced optical waveguides have been investigated since electro-optic crystal with strong electro-optic coefficients became available. A first demonstration was done by Channin [5] in the early 1970s taking advantage of the electro-optic properties of LiTaO₃, but application of a voltage of hundreds of volt was necessary to induce efficient waveguides in a bulk medium. A similar device based on electrodes deposited at the surface of a substrate was later developed by optimization of the electrode design [6] and by choosing a material with a larger electro-optic effect [7].

In the present study, a hybrid structure that takes advantage of domain inversion in LiNbO₃ thin films adhered to silicon is

fabricated to form voltage-operated waveguides. The waveguides properties can be tuned from guiding to antiguiding with a low 10 V amplitude signal. Characterizations performed at telecom wavelengths reveal the good performances of these original hybrid devices that offer an alternative for silicon photonics modulators.

The first stage of the fabrication process is to locally invert ferroelectric domains in a 500 μm thick 4 in. (10.16 cm) diameter Z-cut congruent LiNbO₃ wafer, supplied by Gooch and Housego. To do so, a standard technique involving the application of an intense electric field opposite to the initial Z-axis direction [8] through a photo-resist pattern is used. The mask generating the poling pattern consists in a series of 50 mm long parallel lines 1 mm apart whose width varies from 4 to 16 μm . Observation of the poled wafer with a polarizing microscope reveals the successful poling as witnessed by the presence of 50 mm long narrow stripes oriented along the y axis of the LiNbO₃ wafer. As discussed later in this Letter, the width of the poled stripes is found to be significantly larger than the ones of the mask which is attributed to an overpoling [9]. In a second stage, a 350 nm-thick SiO₂ layer is deposited by ICPECVD onto one face of the poled wafer followed by the sputtering of a 300 nm-thick gold layer. Then, a high flatness 4 in. (10.16 cm) diameter silicon wafer is also coated onto one face with a 300 nm-thick gold layer. The metalized faces of both the PPLN and the silicon wafers are then placed into contact and pressed in an EVG wafer bonding machine. For this bonding process, a pressure of 65 N \cdot cm⁻² is applied under vacuum. This metal diffusion bonding process is realized at room temperature which prevents mechanical stress that could occur due to the dissimilar temperature coefficients of the two wafers. The bonding is finalized by applying a strong pressure to the stack which yields more than 98% of the surface bonded as observed by an ultrasound characterization technique [10]. A 1 mm thick hybrid structure composed of a silicon substrate bonded to a poled LiNbO₃ wafer is thus obtained. The next step is to thin the LiNbO₃ layer down by grinding and polishing to reach a 6 μm thickness. At last, a 350 nm-thick SiO₂ layer is deposited at the surface of the LiNbO₃ film followed by the sputtering of a 300 nm-thick gold electrode. Finally, this hybrid structure is diced with a precision saw to give samples of

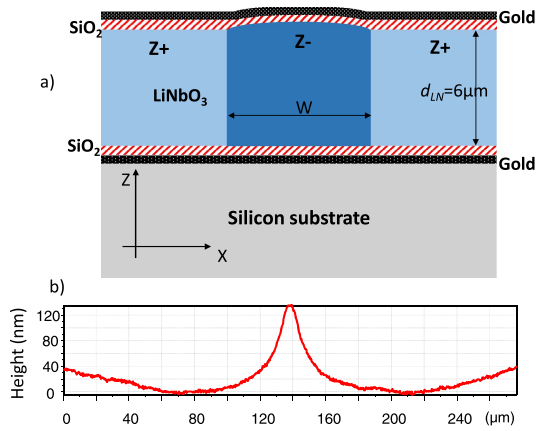


Fig. 1. (a) Schematic cross section of the structure of the voltage-induced waveguides along with (b) the line profile measured with an optical profilometer transversely to a waveguide.

different propagation lengths with polished input and output faces. Each sample thus forms a slab waveguide thanks to the step index between silica ($n_{\text{SiO}_2} = 1.45$) and the $6 \mu\text{m}$ thick LiNbO₃ ($n_{\text{LN}} \approx 2.2$) layer as illustrated in Fig. 1(a). The LiNbO₃ layer is +Z oriented except along the stripes where the domains have been inverted. Characterization of the samples surface flatness with an optical profilometer reveals that the LiNbO₃ film is slightly thicker along these poled stripes. To illustrate this excess thickness, Fig. 1(b) presents the transverse profile measured across a stripe poled with a $6 \mu\text{m}$ wide line of the mask. A 120 nm high and $18 \mu\text{m}$ (FWHM) wide hump is observed. An exhaustive analysis of all poled stripes shows similar profiles but with a height that increases from 100 nm for the narrowest mask lines ($4 \mu\text{m}$) up to 180 nm for the widest lines ($16 \mu\text{m}$). In addition, we found that the hump widths (FWHM) are systematically $12 \mu\text{m}$ wider than the mask line which corroborates a fixed offset due to an overpoling. It suggests that the characteristics of the electrical pulse [9] used for the poling can be optimized. The surface corrugation observed in the -Z oriented area is attributed to the disparate mechanical properties of -Z and +Z oriented LiNbO₃ surfaces [11]. Indeed, -Z surfaces are harder than +Z surfaces which explain that the poled area become slightly thicker than the surrounding areas during the polishing process.

The components described above are then optically characterized. Light from a laser diode emitting at a wavelength of 1550 nm is collimated and linearly polarized. This light beam is focused with a 40 mm focal length lens to be end-fired coupled in the waveguide. Beam overlap with the fundamental mode is optimized to avoid excitation of higher order modes. The image at the output face of the waveguide is formed on a Vidicon camera thanks to a microscope objective. Two electrical wires are then connected to each component. One is attached to the gold layer located at the surface, and the other one is connected to an aluminum electrode deposited on the edge of the component which is in contact with the gold bonding layer. With this configuration, the voltage is directly applied across the SiO₂ and LiNbO₃ layers giving rise to an electric field oriented along the Z axis.

To test the component response, a DC voltage supply is first used. When no driving voltage is present, the light launched in

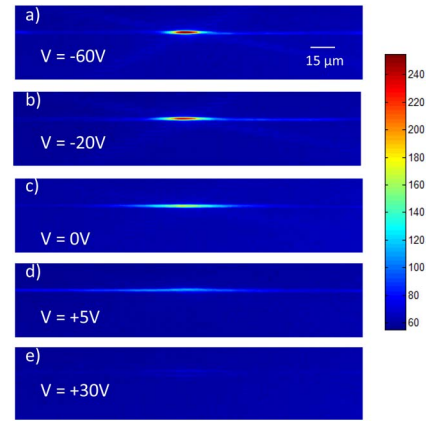


Fig. 2. Output light distribution at the exit face of a 3 cm long waveguide for different applied DC voltage V . Waveguide width W is $16 \mu\text{m}$. Light is extraordinary polarized.

the y direction is weakly guided along the poled stripe thanks to the presence of a rib waveguide induced by the hump present at the surface. To illustrate this effect, Fig. 2(c) depicts the light distribution observed at the exit face of a 3 cm long waveguide whose measured width W is $16 \mu\text{m}$. Note that no coupling to higher order modes is observed experimentally. When the electric potential of the surface electrode is lower than the one of the bonding electrode (negative voltage) the Z-polarized guided mode becomes narrower as observed in Figs. 2(a) and 2(b). This behavior is due to the refractive index change induced by the Z-oriented electric field E_{LN} applied in the LiNbO₃ layer. For a negative voltage, the refractive index increases in the core of the waveguide, while it decreases on both sides. This refractive index deepness Δn along the x axis that depends on light polarization is given by

$$[\Delta n]_{E_{\text{LN}}} = \begin{bmatrix} n_0^3 r_{13} E_{\text{LN}} & 0 & 0 \\ 0 & n_0^3 r_{13} E_{\text{LN}} & 0 \\ 0 & 0 & n_e^3 r_{33} E_{\text{LN}} \end{bmatrix}, \quad (1)$$

where n_0 and n_e are, respectively, the ordinary and extraordinary refractive index of LiNbO₃. r_{33} and r_{13} are coefficients of the LiNbO₃ electro-optic tensor. $n_e = 2.203$, $n_0 = 2.286$ [12], $r_{13} = 9.6 \times 10^{-12} \text{ mV}^{-1}$, $r_{33} = 30.9 \times 10^{-12} \text{ mV}^{-1}$ [13]. A step-index waveguide is thus formed for a negative applied voltage. Note that for a given applied field the refractive index change given by Eq. (1) is twice the one obtained with standard voltage-induced waveguides because it benefits from the two oppositely poled areas.

As expected, the waveguide becomes an antiguide when a positive voltage is applied. The light is repelled from the central part of the waveguide because the index of refraction is lower in the inverted area than on each side as seen in Figs. 2(d) and 2(e). A similar behavior is observed for an X-polarized beam, but the voltage has to be increased accordingly to the lower electro-optic coefficient r_{13} .

To calculate the electric field E_{LN} induced by the voltage V , we consider that the multilayer dielectric structure is composed of SiO₂ and high resistivity LiNbO₃. The line integral relation between the voltage and the static electric field along with the electric displacement continuity then yield

$$E_{\text{LN}} = \frac{-V}{d_{\text{LN}}(1 + d_{\text{SiO}_2}\epsilon_{\text{LN}}/d_{\text{LN}}\epsilon_{\text{SiO}_2})} = \frac{-V}{d_{\text{eff}}}, \quad (2)$$

where $d_{\text{LN}} = 6 \mu\text{m}$ and $d_{\text{SiO}_2} = 0.7 \mu\text{m}$ are, respectively, the thickness of the LiNbO_3 and silica layers, and $\epsilon_{\text{SiO}_2} = 3.9$ and $\epsilon_{\text{LN}} = 35$ are their respective relative dielectric permittivity [14,15]. For the present structure, we find $d_{\text{eff}} = 12 \mu\text{m}$ which is twice the thickness of the LiNbO_3 layer. This effective thickness d_{eff} can be reduced to obtain a larger electric field E_{LN} for a given applied voltage V . Indeed, the SiO_2 layers thickness could be minimized or, preferentially, material with larger dielectric constant than SiO_2 could be used so that the effective thickness d_{eff} approaches d_{LN} . Moreover, a LiNbO_3 film of submicron thickness is also a viable option to improve the component.

The measured mode width as a function of applied voltage is presented in Fig. 3 for extraordinary light. As expected, the behavior is highly nonlinear. For large negative voltage, the guided mode width (FWHM) saturates to a minimum width of approximately $15 \mu\text{m}$ FWHM corresponding to Fig. 2(a) which is close to the measured width of the poled stripe ($16 \mu\text{m}$). It shows that the width of the poled region defines the waveguide width contrary to standard voltage-induced waveguides, where the electric field distribution dictates the waveguide index profile. For the positive applied field, we observe that the guiding effect due to the surface rib is cancelled for an applied voltage of approximately 6 V. Above this latter amplitude, light is repelled from the central region of the waveguide, and the mode width cannot be determined anymore. The tested component is thus in a partial on state in idle position (no applied voltage). Note that a device in low transmission regime (off state) in idle position could have been realized with a slight change in the fabrication process. Indeed, by simply bonding the silicon wafer to the opposite face of the LiNbO_3 wafer, the polishing process would have yielded to the presence of a dip at the surface.

From Eqs. (1) and (2), we find that an applied voltage of 50 V leads to a step index waveguide with a refractive index difference $\Delta n = 1.3 \times 10^{-3}$ between the core and the cladding for extraordinary light. In reference [16], it is found that a waveguide width of approximately $5 \mu\text{m}$ would be best to obtain an optimally confined mode at a wavelength of $1.55 \mu\text{m}$. A better control of the poling process to form narrower waveguides is thus expected to improve the characteristics of these voltage-induced waveguides.

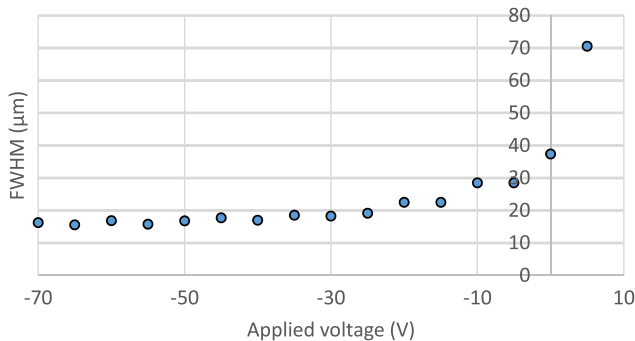


Fig. 3. Mode width versus applied voltage at the exit face of a 3 cm long waveguide versus applied DC voltage. Waveguide width W is $16 \mu\text{m}$.

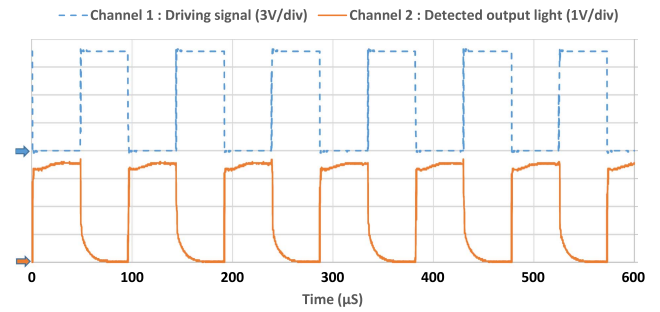


Fig. 4. Chronogram of the transmitted signal (channel 2) detected with a single-mode fiber butt-coupled at the exit face of a 13 mm long waveguide driven by a 10 kHz square positive voltage (channel 1). Channel origins are indicated by arrows placed on the left side.

The large change in mode width depicted in Fig. 3 for an applied voltage between +20 V and -20 V allows envisioning that the tested device can be used as an efficient intensity modulator controlled with a moderate amplitude signal. As a demonstration, a single-mode fiber is butt-coupled to the output of a 13 mm long voltage-controlled waveguide whose other dimensions are similar to the previously tested waveguide. A 50 MHz bandwidth photodiode is connected to the fibered components. Light coupling in the waveguide is still realized with the previous optical spatial set-up. The component transmission response to various electrical signals is then analyzed. As an example, the response to a 10 kHz positive driving square signal is presented in Fig. 4. As expected, the transmitted optical signal is out of phase with the electrical signal. For a positive driving signal of about 10 V amplitude, the contrast between the on and off states reaches 25 dB.

At last, the electrical frequency response of the voltage-controlled waveguide is characterized by applying an AC voltage. The generator is set to apply a weak modulation signal V_{ac} superimposed to a positive offset voltage to work in a linear part of the component transmission response. The response is defined as the ratio of the amplitude of the modulated detected light to the amplitude of the modulation signal. Figure 5 presents the response of the previously used 13 mm long waveguide normalized to the low frequency response. A low-pass frequency response is obtained with an experimental cutoff frequency at 3 dB of 600 kHz. If we consider that LiNbO_3 and SiO_2 are perfectly dielectric (insulator), the equivalent electrical circuit is well described by a series RC model. The resistor value

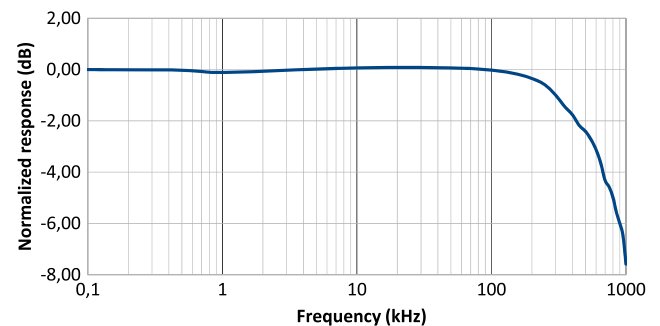


Fig. 5. Normalized frequency response of the 13 mm long voltage-induced waveguide.

R is due to the generator 50 Ω internal resistance, and the capacitor is given by the LiNbO₃ and the SiO₂ layers. The total capacitance C_{eq} can be calculated by the respective capacitance of each layer C_{LN} and C_{SiO_2} :

$$\frac{1}{C_{\text{eq}}} = \frac{1}{C_{\text{LN}}} + \frac{1}{C_{\text{SiO}_2}} = \frac{d_{\text{LN}}}{\epsilon_0 \epsilon_{\text{LN}} S} + \frac{d_{\text{SiO}_2}}{\epsilon_0 \epsilon_{\text{SiO}_2} S}, \quad (3)$$

where S is the surface of the gold electrodes (see Fig. 1). The signal V_{ac} supplied by the generator is applied to this RC circuit, while the transmission variation of the waveguide is proportional to the voltage V_{eff} present across the LiNbO₃ capacitor. The transfer function, defined as $T(f) = V_{\text{eff}}/V$, is thus given by

$$T(f) = \frac{1}{(1 + d_{\text{SiO}_2} \epsilon_{\text{LN}} / d_{\text{LN}} \epsilon_{\text{SiO}_2})(1 + 2\pi RC_{\text{eq}} f)}. \quad (4)$$

$T(f)$ corresponds to the transfer function of a first order low-pass filter with a cutoff frequency $1/2\pi RC_{\text{eq}}$. For the component characterized in Fig. 5, the surface of the electrode is 1.3 cm² which gives a calculated cutoff frequency of about 900 kHz. It is in fair agreement with the experimental results of 600 kHz. The discrepancy may be due to the uncertainties on the characteristics of the deposited SiO₂ layers (thickness and dielectric constant). Moreover, it is important to note that the electrode surface is not ideal because it extends 5 mm on both sides of the tunable waveguide. To gain some bandwidth, the electrode should instead be slightly wider than the waveguide. According to Eq. (3), a 50 μm wide electrode would lead to a frequency cutoff of 200 MHz. Modulators based on voltage-induced waveguides could be achieved with even higher bandwidths by using carefully designed traveling wave electrodes as often used for Mach–Zehnder modulators [17].

The presented voltage-induced waveguides could be at the heart of a variable optical attenuator with a fast response. As stated above, applications such as large bandwidth modulators could also be envisioned. A great advantage of the structure comes from its straightforwardness because it is composed of a single straight waveguide. The simple fabrication process should give high yields at low cost. Alternatives to the described fabrication can be envisioned to simplify it even more. For instance, domain reversal of the LiNbO₃ could be realized after the thinning stage so that the same electrodes could be used for the poling and to apply the electric signal for tuning the waveguides. Optimally aligned electrodes would thus be obtained in a simple fabrication stage. In addition, fabrications of thinner LiNbO₃ films are in progress to both obtain single-mode waveguide and improve the electrical response.

In conclusion, the concept of voltage-controlled waveguides based on the local poling of a LiNbO₃ film has been presented. These components are fabricated by a combination of wafer bonding and grinding/polishing techniques to form few μm

thick locally repoled LiNbO₃ films. Optical characterizations show that the voltage-induced waveguides can be tuned from efficient waveguides to antiguides with a low 10 V amplitude electric signal. This electrical signal can vary the waveguides transmission over more than 25 dB. Electrical bandwidth can reach a few hundred MHz by simple optimization of the electrode dimensions, while faster response could be envisioned with traveling wave electrodes. This first demonstration of an electro-optic induced waveguide with such a manufacturing process opens the way for the fabrication of electrically variable attenuators, fast modulators or even tunable waveguide arrays.

Funding. Région Franche-Comté; Agence Nationale de la Recherche (ANR) (ANR-16-CE24-0024-01).

Acknowledgment. This work was also partly supported by the RENATECH network and its FEMTO-ST MIMENTO technological facility.

REFERENCES

1. J. Liu, M. Beals, A. Pomerene, S. Bernardis, R. Sun, J. Cheng, L. C. Kimerling, and J. Michel, *Nat. Photonics* **2**, 433 (2008).
2. Y. O. Noha, C. H. Leea, J. M. Kima, W. Y. Hwangc, Y. H. Won, H. J. Leea, S. G. Hana, and M. C. Ohd, *Opt. Commun.* **242**, 533 (2004).
3. R. Krähenbühl, M. M. Howerton, J. Dubinger, and A. S. Greenblatt, *J. Lightwave Technol.* **20**, 92 (2002).
4. D. Janner, D. Tulli, M. García-Granda, M. Belmonte, and V. Pruneri, *Laser Photon. Rev.* **3**, 301 (2009).
5. D. J. Channin, *Appl. Phys. Lett.* **19**, 128 (1971).
6. N. A. F. Jaeger and L. Young, *IEEE J. Quantum Electron.* **25**, 720 (1989).
7. J. C. Baumert, C. Walther, P. Buchmann, H. Kaufmann, H. Melchior, and P. Günter, *Appl. Phys. Lett.* **46**, 1018 (1985).
8. E. Courjon, N. Courjal, W. Daniau, G. Lengaigne, L. Gauthier-Manuel, S. Ballandras, and J. Hauden, *J. Appl. Phys.* **102**, 114107 (2007).
9. A. C. Busacca, C. L. Sones, V. Apostolopoulos, R. W. Eason, and S. Mailis, *Appl. Phys. Lett.* **81**, 4946 (2002).
10. S. Ballandras, E. Courjon, F. Bassignot, G. Ulliac, J. Hauden, J. Garcia, T. Laroche, and W. Daniau, in *Ferroelectrics—Applications*, M. Lallart, ed. (InTech, 2011).
11. M. Chauvet, F. Henrot, F. Devaux, L. Gauthier-Manuel, V. Pêcheur, H. Maillotte, F. Bassignot, and B. Dahmani, *J. Opt.* **18**, 085503 (2016).
12. D. E. Zelmon, D. L. Small, and D. Jundt, *J. Opt. Soc. Am. B* **14**, 3319 (1997).
13. E. H. Turner, *Appl. Phys. Lett.* **8**, 303 (1966).
14. F. Giustino, P. Umari, and A. Pasquarello, *Microelectron. Eng.* **72**, 299 (2004).
15. M. Abarkan, M. Aillerie, J. P. Salvestrini, M. D. Fontana, and E. P. Kokanyan, *Appl. Phys. B* **92**, 603 (2008).
16. H. Kogelnik, in *Guided-Wave Optoelectronic*, T. Tamir, ed. (Springer, 1988), p. 19.
17. K. Noguchi, O. Mitomi, and H. Miyazawa, *J. Lightwave Technol.* **16**, 615 (1998).